ARTICLE

Enzyme-Triggered Defined Protein Nanoarrays: Efficient Light-Harvesting Systems to Mimic Chloroplasts

Linlu Zhao, Haoyang Zou, Hao Zhang, Hongcheng Sun, Tingting Wang, Tiezheng Pan, Xiumei Li, Yushi Bai, Shanpeng Qiao, Quan Luo, Jiayun Xu, Chunxi Hou,* and Junqiu Liu*

State Key Laboratory of Supramolecular Structure and Materials, College of Chemistry, Jilin University, 2699 Qianjin Street, Changchun 130012, China

Ⓢ Supporting Information

ABSTRACT: The elegance and efficiency by which chloroplasts harvest solar energy and conduct energy transfer have been a source of inspiration for chemists to mimic such process. However, precise manipulation to obtain orderly arranged antenna chromophores in constructing artificial chloroplast mimics was a great challenge, especially from the structural similarity and bioaffinity standpoints. Here we reported a design strategy that combined covalent and noncovalent interactions to prepare a protein-based light-harvesting system to mimic chloroplasts. Cricoid stable protein one (SP1) was utilized as a building block model. Under enzyme-triggered covalent protein assembly, mutant SP1 with tyrosine (Tyr) residues at the designated sites can couple together to form nanostructures. Through controlling the Tyr sites on the protein surface, we can manipulate the assembly orientation to respectively generate 1D nanotubes and 2D nanosheets. The excellent stability endowed the self-assembled protein architectures with promising applications. We further integrated quantum dots (QDs) possessing optical and electronic properties with the 2D nanosheets to fabricate chloroplast mimics. By attaching different sized QDs as donor and acceptor chromophores to the negatively charged surface of SP1-based protein nanosheets *via* electrostatic interactions, we successfully developed an artificial light-harvesting system. The assembled protein nanosheets structurally resembled the natural thylakoids, and the QDs can achieve pronounced FRET phenomenon just like the chlorophylls. Therefore, the coassembled system was meaningful to explore the photosynthetic process *in vitro*, as it was designed to mimic the natural chloroplast.

KEYWORDS: protein nanostructures, protein assembly, light-harvesting, quantum dot, chloroplast mimic
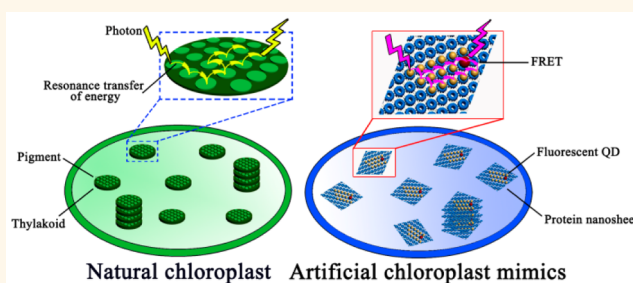
I n nature, efficient transfer of energy in the photosynthetic process was achieved through the manipulation of antenna chromophores that adopt hierarchically ordered arrangements.[1−4] The most extraordinary part of this process is the chloroplast, an intriguing molecular machine found in plant cells and eukaryotic algae that contains the tightly stacked thylakoids and regulated aligned chlorophylls to construct highly efficient photosynthetic systems and thus maintain the whole life activity.[5−8] Significantly, the sheet-like thylakoids play essential roles in photosynthesis, on which the pigments adopt a fixed distance and orientation to facilitate their high energy-transfer efficiency. Following the wisdom of nature, mimicking natural light-harvesting systems is one of the most exciting areas in exploring solar energy conversion and utilization,[9−13] especially its potential ability in solar cells,[14] optical sensors,[15] photocatalysis,[16] and light-emitting materials.[17] A variety of scaffolds have been utilized to realize efficient energy-transfer processes.[18−22] However, how to develop a versatile scaffold to make the fluorescent chromophores arrange orderly for constructing highly efficient light-harvesting mimics without time-consuming synthesis or energy loss by contact quenching is a great challenge.

A desirable scaffold was protein assemblies,[23−26] which possess an inherent affinity to the real nature in mimicking light-harvesting processes. Our preceding studies demonstrated that ring-shaped proteins can assemble into relatively simple one-dimensional (1D) nanowires with fluorescent donor and acceptor chromophores orderly arranged to construct an artificial light-harvesting system.[27,28] Nevertheless, the one-way transfer of energy on this nanowire restricted its

Scheme 1. Schematic representation of the formation of protein nanotubes or nanosheets *via* enzyme catalysis. (a) Vertical modification on the top and bottom surfaces of SP1 to obtain the SP1A84Y variant. Under single-enzyme (HRP) catalysis, Tyr residues at the 84 site of SP1 coupled along the C_6 symmetry axis to generate 1D nanotubes. (b) Horizontal modification at the periphery of SP1 to obtain the SP1S98Y variant. It grew isotropically along the protein plane to form 2D nanosheets in the presence of HRP and H_2O_2. Moreover, dual enzyme-cooperative catalysis can also obtain these nanostructures with high stability. The frame is the mechanism of the coupling of the Tyr residues to achieve assembly.
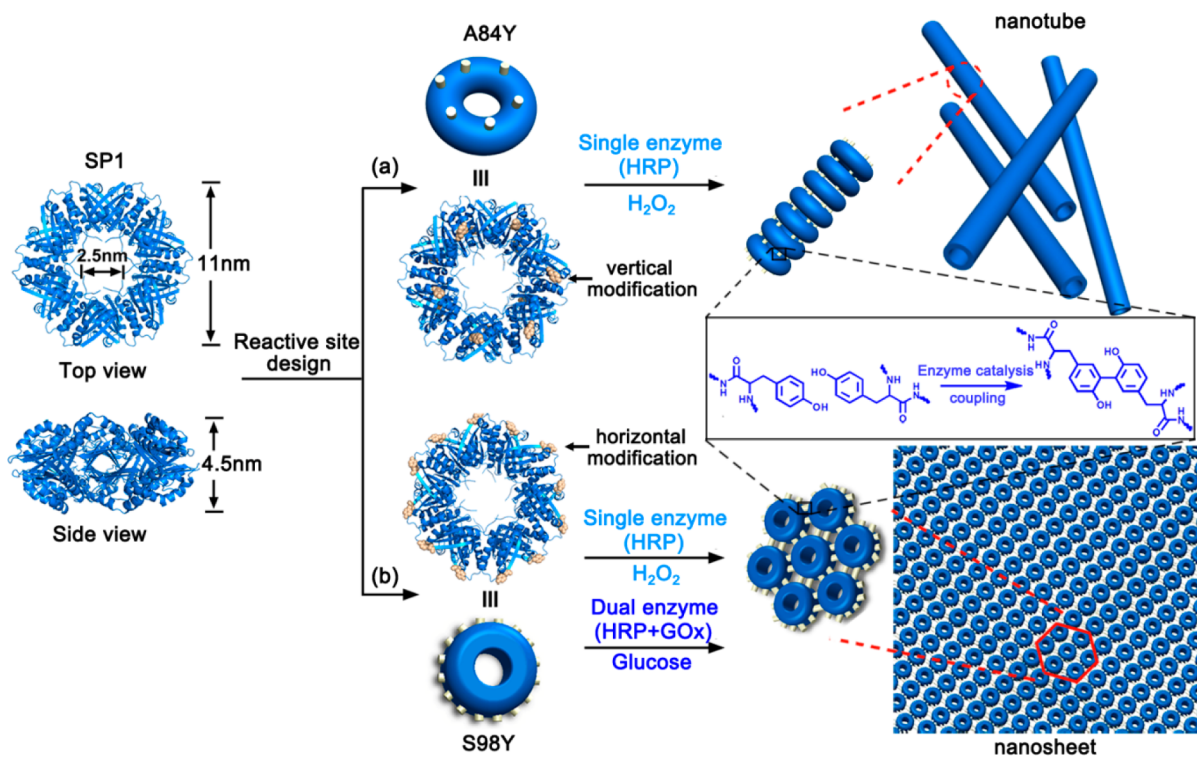
practicability; that is, once one of the fluorescent chromophores failed to work, the entire energy-transfer process would be cut off. In this regard, the construction of chloroplast mimics utilizing protein assemblies that can offer multidirectional energy-transfer paths was highly desirable. Notably, nature creates photosynthetic centers depending on the integration of covalent and noncovalent interactions. Covalent nanostructures have excellent stability, and noncovalent assemblies allow a "self-checking" process to achieve an ordered arrangement. Inspired by these features, here we established a strategy, that is, an enzyme-triggered covalent protein assembly, to precisely assemble the fragile proteins into periodically arranged 2D nanosheets. The assembled protein nanostructures possessed great potential to well-distribute the fluorescent chromophores.

To construct the self-assembled chloroplast mimics, we designed hybrid architectures utilizing protein nanostructures and highly efficient fluorescent molecules. Here we chose stable protein one (SP1) as our model protein. It is a natural dodecamer with 12 identical subunits bound to each other *via* hydrophobic interactions, forming a double-layered six-membered ring and related by a pseudo-6-fold axis (C_6 symmetry).[29,30] In addition, SP1 has extremely high thermal and chemical stability, which is a quite advantageous feature for protein assembly. It is generally known that tyrosine (Tyr) residues can achieve coupling in horseradish peroxidase (HRP)-catalyzed systems,[31,32] which facilitates this methodology to be applied in fabricating protein architectures for Tyr residues, being one of the constituents in proteins. Notably, computer simulations showed that the original Tyr residues in SP1 were distributed inside and did not participate in the HRP-catalyzed

assembly process; that is, we can introduce Tyr residues in the target site to guide the assembly orientation. Due to the peculiar symmetric structure, ring-shaped SP1 was predicted to grow isotropically when the reactive Tyr residues were symmetrically introduced to the periphery of SP1.

By exploiting HRP-triggered covalent protein assembly, we anticipated the fabrication the sheet-like protein nanoarrays that structurally resembled the thylakoids in natural chloroplasts. The obtained architectures were expected to possess excellent stability due to this subtle assembled methodology. Furthermore, integration of quantum dots (QDs) possessing optical or electronic properties with engineered biological scaffolds or templates can yield excellent nanoscale systems.[33−36] We thus labeled different sized QDs, a kind of semiconductor with size-dependent fluorescence emission, as donor and acceptor chromophores on the surface of the assembled protein nanosheets *via* electrostatic interactions. The ordered distribution of these QDs in the assembled system enabled them to exert the same function as chlorophylls in chloroplasts. An energy-transfer process can be achieved from donors to the nearby acceptor chromophores. Therefore, the coassembled system was meaningful to explore the photosynthetic process *in vitro* as it was designed to mimic the natural chloroplast.

RESULTS AND DISCUSSION

In order to identify the feasibility of this enzyme-triggered nanotechnology on the protein assembly system, we first endeavored to construct relatively simple one-dimensional

(1D) SP1 nanotubes (Scheme 1a). By virtue of computer aid, we selected Ala84 on the top and bottom surfaces and then obtained the SP1A84Y variant successfully. In the presence of H_2O_2 and HRP, the mutant axial Tyr residues were supposed to react with the other Tyr residues of adjacent SP1 variants to guide their growth along the C_6 symmetry axis to form linear protein nanotubes. The formation of SP1A84Y assemblies was preliminarily studied by dynamic light scattering (DLS) with increasing hydrodynamic radius upon HRP and H_2O_2 addition (Figure S4). For further exploring the internal interaction behavior, we utilized MALDI-TOF mass spectrometry to characterize the assemblies (Figure S5a). The obtained SP1 dimer was strong proof of the covalent cross-linking between the proteins compared to the only SP1 monomer observed in SP1A84Y as a control. Upon HRP catalysis, it underwent covalent coupling into dityrosine and further growing along the symmetry axis to form nanostructures. Fortunately, the generated Tyr-coupled product was a fluorescent dimer, which can serve as an effective probe to monitor the enzyme-triggered covalent assembly process in the fluorescence spectrum.[37,38] Emission spectra showed that a characteristic peak appeared after a certain time of adding H_2O_2 and HRP to the assembly system, and the intensity of the peak increased as time went on (Figure S5b).

The morphology of the enzyme-triggered protein assemblies was observed by tapping-mode atomic force microscopy (AFM). As was shown in Figure 1a,c, ring-shaped SP1 packed
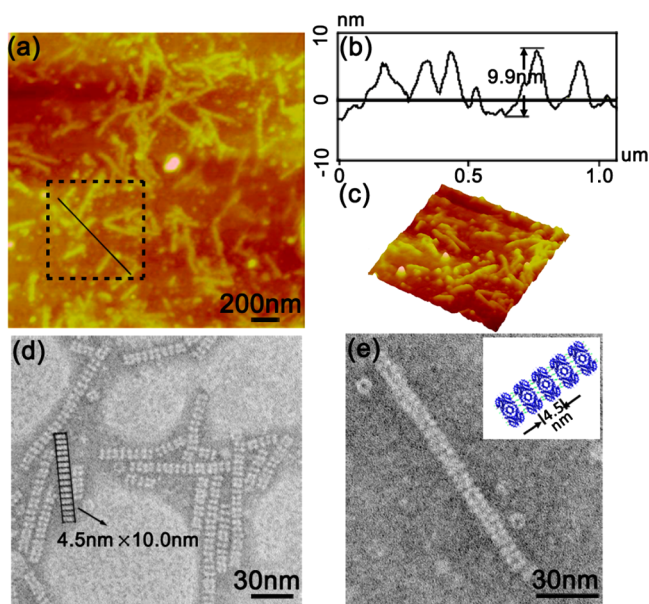
Figure 1. Morphologies of SP1A84Y nanostructures. (a) AFM images of the 1D linear protein assemblies. (b) Height profile of the black line in (a). (c) 3D images of the squares in (a). (d) TEM characterization of the protein nanotubes. (e) TEM images of a single protein nanotube. Inset is the model of the SP1A84Y nanotube stacked under HRP catalysis. [SP1A84Y] = 0.05 mg/mL.

together to form linear nanostructures several hundred nanometers in length upon addition of HRP and H_2O_2. The uniform height (~10 nm) of the protein architectures was consistent with that of the crystal structure (11 nm) (Figure 1b). To further explore the detailed structure of the assemblies, transmission electron microscopy (TEM) was used for this purpose (Figure 1d). We can find that SP1 rings were all

arranged parallel to the C_6 axis to form the nanotubes, which validated our hypothesis of the growth mechanism that the Tyr residues on the top and bottom surfaces of SP1A84Y realized coupling between interprotein interactions under enzyme catalysis (Figure 1e). The data above clearly identified the obtained nanotubes with our original design and at the same time confirmed the feasibility of enzyme-triggered nano-technology in catalyzing a protein system to achieve super-structures.

As the protein nanotubes have been successfully constructed based on this HRP-triggered strategy, we believed that 2D architectures can also be obtained by mutation at the periphery of the SP1 ring. After analyzing the SP1 structural model with Pymol, we found that site Ser98 at the periphery was a quite favorable choice for the mutant design, as it provided the suitable distance to form dityrosine linkages between adjacent SP1 rings. In addition, it also facilitated the protein−protein spatial charge complementation in lateral directions. Under HRP catalysis, the 12 lateral Tyr residues per SP1 coupled with others isotropically to finally generate 2D single-layer nano-sheets. Due to the isotropically growing pattern and special dodecamer ring-shaped structure of the building blocks, the nanosheets should present hexagonal packing similar to the natural protein crystal (Scheme 1b).

Compared with the 1D protein nanotubes constructed by SP1A84Y, the change of the mutant site in SP1 led to a distinctly different morphology. Remarkably, the SP1S98Y with Tyr residues at the periphery grew in lateral directions to ultimately form highly ordered 2D layer-like nanostructures several hundred nanometers in size (Figure 2a). The uniform height of the morphology (~4 nm) was clearly indicative of the single-layer nanostructures (Figure 2c,d), as it was well consistent with the theoretical size of the ring-shaped SP1 (height 4.5 nm). Furthermore, TEM data well supported the AFM findings. Figure 2b showed closely packed, extended sheet morphologies composed of regular repeating SP1 units. We can clearly find that these SP1 rings formed the hexagonal packing nanosheets, which coincided with our prediction of mutant Tyr98 coupled with each other to grow in six lateral directions isotropically under HRP catalysis. All the results obtained proved the successful construction of 2D protein nanosheets based on enzyme catalysis. Furthermore, through controlling the charge distribution on the top and bottom surfaces of SP1 by altering pH, we can regulate the single-layer nanosheets into multilayer structures. As the isoelectric point (pI) was about 4.3, at relatively high pH (pH = 7.5), monolayer nanosheets can be obtained due to the Coulomb repulsion between 2D nanosheets as a large amount of negative charges was distributed on the top and bottom surfaces of SP1S98Y (Figure S12a,c). However, at low pH (pH = 4.75), which is quite near the pI, protein surfaces can hardly possess enough negative charges to separate the nanosheets, and thus multilayer nanosheets were formed (Figure S12b,d).

To improve the bioaffinity of the assembly system, we expanded the single-enzyme catalysis to a dual-enzyme cooperative mechanism to avoid the direct addition of H_2O_2 to the system. HRP and glucose oxidase (GOx) were selected to cocatalyze the protein assembly with glucose addition. HRP catalyzed H_2O_2, which was produced by GOx, catalyzing glucose to oxidize the tyrosine residues in SP1S98Y to achieve assembly (Figure 2e). Figure 2f shows the obtained morphology in AFM, where flat sheet structures were observed of several hundred nanometers in size. The remarkable
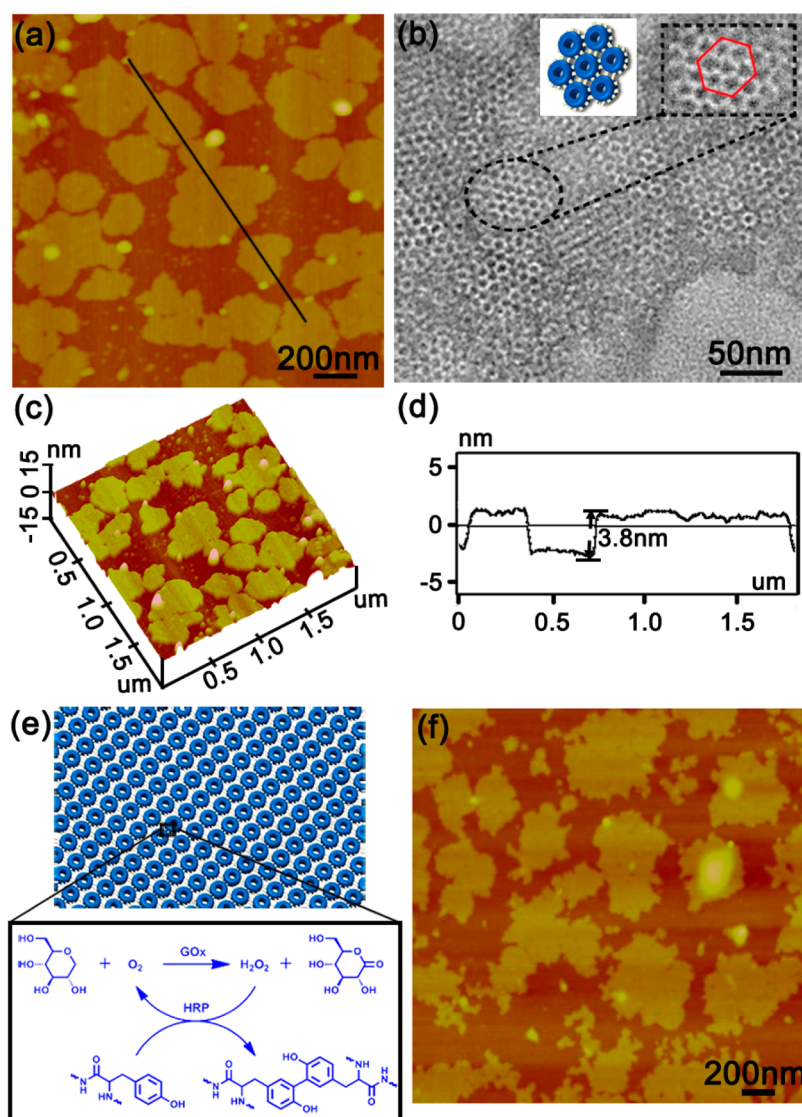
Figure 2. Morphologies of SP1S98Y nanostructures. (a) AFM images of the 2D layered protein architectures. (b) TEM characterization of the protein nanosheets (inset: hexagonal packing model of the protein nanosheets). (c) 3D images of the squares in (a). (d) Height profile of the black line in (a). (e) Mechanism of dual-enzyme-catalyzed protein architectures. (f) AFM images of the 2D nanosheets obtained from dual-enzyme catalysis. [SP1S98Y] = 0.05 mg/mL, pH = 7.5.

predominance of this enzyme-triggered strategy *via* covalent interactions compared with those based on conventional weak interactions was mainly reflected in the structural stability. Heat treatment up to 70 °C of the assembly sample for 30 min was characterized by AFM (Figure S13). As the temperature increased, we found that the nanosheets still maintained the original pattern even at high temperature. All in all, the enzyme-triggered nanosheets possessed a high thermal stability to keep their morphologies unchanged even at high temperature. This excellent feature endowed the self-assembled protein architectures with promising applications.

In plants and algae, chloroplasts maintain the whole life activity by achieving an efficient energy-transfer process from donor to acceptor chromophores. However, the main challenge to construct highly efficient chloroplast mimics is how to make the pigments arrange orderly on the "thylakoids", thus to conduct effective energy transfer rather than self-quenching inactivation. We think the assembled 2D protein nanosheets can serve as an ideal scaffold for mimicking chloroplasts, not

only for their structural similarity with the thylakoids but also for the ordered arrangements constructed of ring-shaped protein. Owing to the negatively charged surface and regular distributed central hole (Figure 3a), the protein nanosheets offer suitable distances for attaching positively charged QDs to construct complete chloroplast mimics. In view of the spatial complement, we chose surface-aminated CdTe QD1 with a diameter of about 3 nm and QD2 of about 5 nm (Figure 3b) to coassemble with the protein nanosheets *via* electrostatic interactions (Figure 3c). As the QDs possess multiple superior properties such as photostability, relatively high quantum yield (QY), size-dependent fluorescence emission, and tunable optical properties, we anticipate that the absorbing energy can be transferred on the assembled protein nanosheets with QD1 and QD2 as donors and acceptors, respectively. Notably, we designed the coassembled system to mimic the natural chloroplast from both the structural similarity and the light-harvesting properties (Figure 3d).
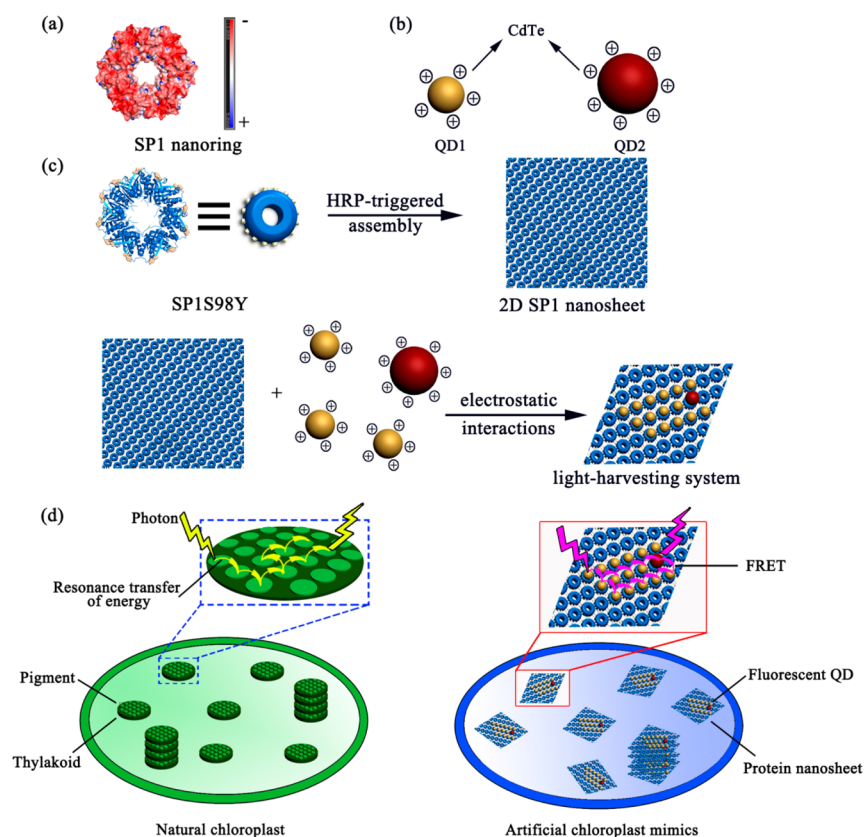
Figure 3. (a) SP1 nanoring structure with charge distribution on the surface. The red color is for negative charges, and the blue color is for positive charges. (b) Two kinds of CdTe QDs were capped with mercaptoethylamine (positive charges), where the diameters of QDs are about 3−4 nm for QD1 and 5−6 nm for QD2. (c) Construction of a light-harvesting system based on electrostatic interactions of the 2D protein nanosheets formed by HRP-triggered covalent assembly and two different sized fluorescent QDs. (d) Schematic representation of the comparison of natural chloroplast and artificial chloroplast mimics based on the coassembly of protein nanosheets and QDs.
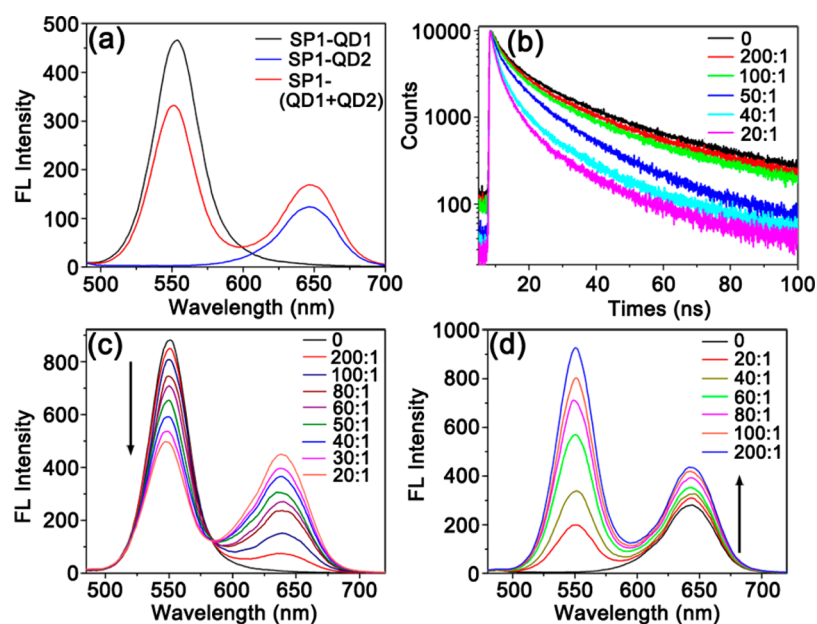
Figure 4. Fluorescence properties of functional protein nanosheets constructed by SP1S98Y-based nanosheets and QDs. (a) FL spectra of donor QD1 with SP1S98Y-based nanosheets (black line) and acceptor QD2 with the nanosheets (blue line) in aqueous solutions and of their mixture solution (red line). (b) Donor fluorescence decay curves in the absence (black line) and in the presence of different concentrations of acceptor. $[QD1] = 50\ \mu M$. (c) FRET spectra of the coassembly (SP1S98Y-based nanosheets-QD1-QD2) with various amounts of acceptor QD2. $[QD1] = 50\ \mu M$. (d) FRET spectra of the coassembly system with various amounts of donor QD1. $[QD2] = 0.5$ mM. (For all the systems: $[SP1S98Y] = 0.15$ mg/mL, pH = 7.5, $\lambda_{ex} = 420$ nm.)

In order to explore the energy-transfer process, QD1 and QD2 were mixed well first and then added to the sheet assemblies, where the positively charged QDs can be orderly arranged on the surface of the assembled nanosheets *via* electrostatic interactions. Figure 4a shows the change of the fluorescence intensity when QD1 and QD2 were coassembled with the nanosheets compared with QD1/QD2 assembled with the nanosheets alone, respectively. There was an obvious decrease in the emission intensity of the donor QD1 at 550 nm but a clear increase of the acceptor QD2 at 650 nm, which illustrated the occurrence of a fluorescence resonance energy transfer (FRET) phenomenon between these two QDs on the nanosheets. In order to explore the detailed FRET effect, we further studied the lifetime of the donor QD1 in this coassembly system. It showed a significant change in the presence of the acceptor QD2 compared to the donor QD1 alone (Figure 4b). The average lifetime ($\langle \tau \rangle$) of QD1-SP1S98Y-based nanosheets was 25.0 ns, while it was modified distinctly with the addition of QD2 and even decreased to 11.1 ns, which strongly indicated the possibility of energy transfer from QD1 to QD2 on the 2D nanosheets. Besides, it was meaningful to calculate the energy-transfer efficiency of donor to acceptor according to donor lifetime variation, and the value was 56% at a ratio of 20:1 for QD1 to QD2.

With an increasing concentration of QD2 in the coassembly system, the emission intensity for donor QD1 at 550 nm was gradually attenuated and that for acceptor QD2 at 650 nm was enhanced when excited at 420 nm (Figure 4c). The attenuation of QD1 emission accounted for the fact that the absorbing energy was transferred from QD1 to QD2 on the assembled nanosheets. In comparison, no energy transfer was found without the 2D SP1S98Y-based nanosheets, which could be attributed to the monodispersed nature of the QDs owing to electrostatic repulsion (Figure S14). On the contrary, the increase in QD1 concentration caused the enhancement of the emission intensity at both 550 and 650 nm, which also reflected a pronounced FRET effect (Figure 4d). Significantly, TEM characterization was used to further validate the energy-transfer process. A mixture of QD1 and QD2 with a number proportion of 40:1 was added to the prepared SP1S98Y-based nanosheets. The constructed light-harvesting system was then incubated for 1 h. From the measurement of diameters of the dots sitting on the center of the SP1 nanoring on TEM (3.0 and 5.0 nm, consistent with the size of QD1 and QD2, respectively), we confirmed the attachment of QDs to the center of the SP1 protein. There were mainly two types of arrangements of QDs on the nanosheets from TEM images (Figure 5a). One was that "small" QDs (donor QD1) closely packed on the surface of SP1S98Y-based nanosheets orderly, and the other type referred to multiple "small" QDs arranged adjacent to a few "big" QDs (acceptor QD2) on the sheet structures. Combined with previous results, it was possible that the absorbing energy can be transferred through successive donor-to-donor events and then shuttle the collected energy to the nearby acceptor QD2 with high energy-transfer efficiency (Figure 5b). The coassembled system was designed by mimicking both the structural feature and light-harvesting properties of the natural chloroplast, which was meaningful to explore the photosynthesis process *in vitro*. We believe that 3D nanoarrays constructed by protein assembly also hold great potential in light harvesting as the curved surface structures of 3D architectures are likely to broaden the energy-transfer path of the fluorescent chromophores.
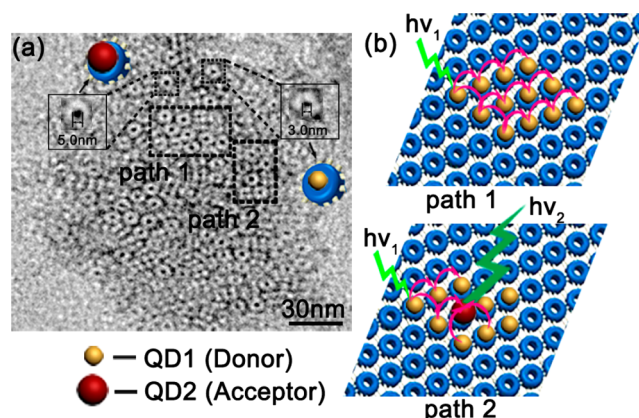
Figure 5. (a) TEM images of SP1S98Y-based nanosheets-QD1-QD2 coassembly, where the number proportion of QD1-QD2 is 40:1. Schematic presentations of the two QDs attached to the surface of the SP1S98Y are also shown, respectively. (b) Schemes of the energy-transfer process on the protein nanosheets: the absorbing energy can be transferred through successive donor-to-donor events (path 1) and then shuttle the collected energy to the nearby acceptor QD2 (path 2).

CONCLUSION

In summary, we have successfully constructed chloroplast mimics by integrating enzyme-triggered nanotechnology and electrostatic supramolecular interactions. The defined 2D protein architectures based on HRP-induced covalent assembly exhibited excellent stability and significant ordered ring-shaped packing. Furthermore, by means of attaching fluorescent donors (QD1) and acceptors (QD2) to the surface of the 2D protein nanosheets *via* electrostatic interactions, we fabricated complete chloroplast mimics, which possessed not only structural similarity to the natural chloroplast but also the ability to efficiently achieve light-harvesting ability. The ordered arrangements of the QDs on the nanosheets exhibited a pronounced FRET phenomenon from multiple successive donors (QD1) to the adjacent acceptors (QD2). The constructed chloroplast mimic can serve as a versatile scaffold for energy transfer and lay the foundation for practical applications such as hydrogen production and photodynamic therapy.

EXPERIMENTAL SECTION

Construction of Plasmids Encoding for SP1 (A84Y) and SP1 (S98Y). Construction of pET22b plasmids containing SP1 (A84Y) and SP1 (S98Y) protein genes, respectively, can be realized by site-directed mutagenesis. The primers a1 (GATTCTTACGCTCTTG-CTGCATTT), b1 (AGCAAGAGCGTAAGAATCGAGGTACT) for the 84 site and a2 (CCTACTTTGTATCAGCGTCTTG), b2 (AAGACGCTGATACAAAGTAGGC) for the 98 site used in site-directed PCR were synthesized by Sangon Biotech. The plasmid pET22b-SP1 provided by Professor Oded Shoseyov (The Hebrew University of Jerusalem, Israel) was used as the template for PCR cloning to obtain the mutant plasmids pET22b-SP1 (A84Y) and pET22b-SP1 (S98Y), respectively. The resulting plasmids were confirmed by DNA sequencing and then transformed into *Escherichia coli* BL21 (DE3) for protein expression.

Overexpression and Purification. The *E. coli* BL21 (DE3) strains were cultured in Luria broth (LB) containing 100 μg/mL ampicillin with shaking at 37 °C. When OD600 reached 0.8, 1 mM isopropyl β-D-1-thiogalactopyranoside (IPTG) was added to the SP1 (A84Y) LB and 0.2 mM IPTG was added to the SP1 (S98Y) LB to induce protein expression. The cells were incubated at 28 °C for 4 h

and then harvested by centrifugation at 8000 rpm for 15 min. Resuspended in 20 mM Tris-HCl buffer (pH 8.0), the cells were sonicated to extract the protein. The insoluble pellets were separated by centrifugation at 15 000 rpm for 30 min. For purification, soluble mutant proteins SP1 (A84Y) and SP1 (S98Y) were first heated at 85 °C and centrifuged at 15 000 rpm for 30 min. The supernatant was further purified by a DEAE ion-exchange column in 20 mM Tris-HCl buffer. The eluted solution was a gradient of NaCl from 100 to 500 mM, and the target protein was eluted in 500 mM NaCl. For further purification, the protein was loaded into a Sephadex G75 with 20 mM PBS buffer (pH 7.4). The obtained solution was dialyzed to remove the salts. The purified proteins were characterized by SDS-PAGE gel electrophoresis (Figure S2), and the molecular weights of the mutants were performed using MALDI-TOF mass spectrometry (Figure S3).

Preparation of CdTe QDs of Different Sizes. The preparation of aqueous CdTe QDs is completely in one pot. Typically, 8 mL of 100 mM $CdCl_2$ aqueous solution, 64 mL of water, 142 μL of 3-Mercaptopropionic acid (purchased from Sigma-Aldrich), 8 mL of 20 mM Na_2TeO_3 aqueous solution, and 100 mg of $NaBH_4$ were added in a conical flask in turn and maintained in the dark at room temperature for 48 h. The concentration of precursors was 10 mM referring to Cd^{2+}, and the molar ratio of $Cd^{2+}/MPA/TeO_3^{2-}/NaBH_4$ was 1:2.0:0.2:3.4. The resultant precursor solutions were refluxed at 100 °C to maintain the growth of QDs. Their sizes increased with reflux duration. QD1 was obtained after 40 min; QD2 after 8 h. After preparation, the QD solution was centrifuged at a speed of 8000 rpm with the addition of isopropyl alcohol to remove superfluous salts and MPA. The precipitated QDs were then redissolved in deionized water.

Enzyme-Triggered Covalent Protein Self-Assembly and Fluorescence Assays. Freshly prepared SP1 (A84Y) or SP1 (S98Y) was dissolved in Milli-Q water at a concentration of 0.15 mg/mL, and 2.4×10^{-5} M H_2O_2 and 5 μg/mL HRP were added to the solution of 20 mM PBS (pH 7.5). The mixture was then incubated overnight at room temperature. It was reported that Try residues could be oxidized to a fluorescent dimer by H_2O_2 under the catalysis of HRP. Under the optimum experimental conditions, the excitation and emission wavelengths of protein assemblies were 330 and 423 nm, respectively. Thus, the assembly process and HRP-catalyzed mechanism were identified and monitored by fluorescence emission spectrum. As time went on, the ratio of protein assemblies became larger and ultimately approached a maximum, which can be reflected on the spectrum. All fluorescent measurements were carried out on a Shimadzu RF-5301 PC spectrofluorimeter.

Dynamic Light Scattering. DLS measurements were made on a Malvern Instrument Zetasizer Nano ZS instrument, and each measurement was carried out three times at 25 °C. Samples were all dissolved in Milli-Q water and tested at different times to monitor the growth process of the nanostructures.

Atomic Force Microscopy. Samples were prepared by dropping 10 μL of a 0.05 mg/mL solution of protein assemblies on a freshly prepared hydroxylated silicon wafer for 10 min, washing with Milli-Q water, and drying under air. The measurements were performed on a Nanoscope III controller (Veeco Metrology, Santa Barbara, CA, USA) using tapping mode with a SiN_4 tip.

Transmission Electron Microscopy. The images were recorded by a JEM-2100F instrument with an accelerating voltage of 120 kV. Samples were prepared on Formvar carbon-coated copper grids by placing a 4 μL drop of a 0.05 mg/mL solution of protein assemblies on it. Samples were kept for 10 min and then drawn away by pipet. Samples were negatively stained by adding 4 μL of stain (2% sodium phosphotungstate in Milli-Q water) onto the grid for 40 s, and then the excess strain was removed. The samples were dried under air flow overnight before imaging.

ASSOCIATED CONTENT

Ⓢ Supporting Information

The Supporting Information is available free of charge on the ACS Publications website at DOI: 10.1021/acsnano.6b07527.

Schematic representation of mutant SP1; expression and characterization (SDS-PAGE, MALDI-TOF, CD spectra) of SP1 variants; MALDI-TOF mass spectrometry and fluorescence spectrum of enzyme-triggered protein assemblies; DLS, AFM, and TEM of SP1/QDs complexes (PDF)

AUTHOR INFORMATION

Corresponding Authors
*E-mail: chunxihou@jlu.edu.cn.
*E-mail: junqiuliu@jlu.edu.cn.

ORCID Ⓞ
Hao Zhang: 0000-0002-2373-1100
Junqiu Liu: 0000-0002-8922-454X

Notes
The authors declare no competing financial interest.

REFERENCES

(1) McDermott, G.; Prince, S. M.; Freer, A. A.; Hawthornthwaite-Lawless, A. M.; Papiz, M. Z.; Cogdell, R. J.; Isaacs, N. W. Crystal Structure of an Integral Membrane Light-Harvesting Complex from Photosynthetic Bacteria. *Nature* **1995**, *374*, 517−521.

(2) van Oijen, A. M.; Ketelaars, M.; Köhler, J.; Aartsma, T. J.; Schmidt, J. Unraveling the Electronic Structure of Individual Photosynthetic Pigment-Protein Complexes. *Science* **1999**, *285*, 400−402.

(3) Hu, X. C.; Damjanovic, A.; Ritz, T.; Schulten, K. Architecture and Mechanism of the Light-Harvesting Apparatus of Purple Bacteria. *Proc. Natl. Acad. Sci. U. S. A.* **1998**, *95*, 5935−5941.

(4) Scholes, G. D.; Fleming, G. R.; Olaya-Castro, A.; van Grondelle, R. Lessons from Nature about Solar Light Harvesting. *Nat. Chem.* **2011**, *23*, 763−774.

(5) Croce, R.; van Amerongen, H. Natural Strategies for Photosynthetic Light Harvesting. *Nat. Chem. Biol.* **2014**, *10*, 492−501.

(6) Hoober, J. K.; Eggink, L. L.; Chen, M. Chlorophylls, Ligands and Assembly of Light-Harvesting Complexes in Chloroplasts. *Photosynth. Res.* **2007**, *94*, 387−400.

(7) Scholes, G. D.; Fleming, G. R. Energy Transfer in Photosynthesis. *Adv. Chem. Phys.* **2005**, *132*, 57−129.

(8) Munekage, Y. N. Light Harvesting and Chloroplast Electron Transport in NADP-Malic Enzyme Type C_4 Plants. *Curr. Opin. Plant Biol.* **2016**, *31*, 9−15.

(9) Peng, H. Q.; Chen, Y. Z.; Zhao, Y.; Yang, Q. Z.; Wu, L. Z.; Tung, C. H.; Zhang, L. P.; Tong, Q. X. Artificial Light-Harvesting System Based on Multifunctional Surface-Cross-Linked Micelles. *Angew. Chem., Int. Ed.* **2012**, *51*, 2088−2092.

(10) Chen, P. Z.; Weng, Y. X.; Niu, L. Y.; Chen, Y. Z.; Wu, L. Z.; Tung, C. H.; Yang, Q. Z. Light-Harvesting Systems Based on Organic Nanocrystals To Mimic Chlorosomes. *Angew. Chem.* **2016**, *128*, 1−6.

(11) Liu, K.; Xing, R. R.; Li, Y. X.; Zou, Q. L.; Möhwald, H.; Yan, X. H. Mimicking Primitive Photobacteria: Sustainable Hydrogen Evolution Based on Peptide−Porphyrin Co-Assemblies with a Self-Mineralized Reaction Center. *Angew. Chem., Int. Ed.* **2016**, *55*, 12503−12507.

(12) Zou, Q. L.; Liu, K.; Abbas, M.; Yan, X. H. Peptide-Modulated Self-Assembly of Chromophores toward Biomimetic Light-Harvesting Nanoarchitectonics. *Adv. Mater.* **2016**, *28*, 1031−1043.

(13) Liu, K.; Xing, R. R.; Chen, C. J.; Shen, G. Z.; Yan, L. Y.; Zou, Q. L.; Ma, G. H.; Möwald, H.; Yan, X. H. Peptide-Induced Hierarchical Long-Range Order and Photocatalytic Activity of Porphyrin Assemblies. *Angew. Chem.* **2015**, *54*, 500−505.

(14) Miyasaka, T. Toward Printable Sensitized Mesoscopic Solar Cells: Light-Harvesting Management with Thin TiO_2 Films. *J. Phys. Chem. Lett.* **2011**, *2*, 262−269.

(15) McQuade, D. T.; Hegedus, A. H.; Swager, T. M. Signal Amplification of a "Turn-on" Sensor: Harvesting the Light Captured by a Conjugated Polymer. *J. Am. Chem. Soc.* **2000**, *122*, 12389−12390.

(16) Gust, D.; Moore, T. A.; Moore, A. L. Mimicking Photosynthetic Solar Energy Transduction. *Acc. Chem. Res.* **2001**, *34*, 40−48.

(17) Mayr, T.; Borisov, S. M.; Abel, T.; Enko, B.; Waich, K.; Mistlberger, G.; Klimant, I. Light Harvesting as a Simple and Versatile Way to Enhance Brightness of Luminescent Sensors. *Anal. Chem.* **2009**, *81*, 6541−6545.

(18) Wasielewski, M. R. Self-Assembly Strategies for Integrating Light Harvesting and Charge Separation in Artificial Photosynthetic Systems. *Acc. Chem. Res.* **2009**, *42*, 1910−1921.

(19) Balzani, V.; Bergamini, G.; Ceroni, P.; Vögtle, F. Electronic Spectroscopy of Metal Complexes with Dendritic Ligands. *Coord. Chem. Rev.* **2007**, *251*, 525−535.

(20) Ajayaghosh, A.; Praveen, V. K.; Vijayakumar, C. Organogels as Scaffolds for Excitation Energy Transfer and Light Harvesting. *Chem. Soc. Rev.* **2008**, *37*, 109−122.

(21) Aratani, N.; Kim, D.; Osuka, A. Discrete Cyclic Porphyrin Arrays as Artificial Light-Harvesting Antenna. *Acc. Chem. Res.* **2009**, *42*, 1922−1934.

(22) Choi, M. S.; Aida, T.; Yamazaki, T.; Yamazaki, I. A Large Dendritic Multiporphyrin Array as a Mimic of Bacterial Light-Harvesting Antenna Complex: Molecular Design of an Efficient Energy Funnel for Visible Photons. *Angew. Chem.* **2001**, *113*, 3294−3298.

(23) Sakai, F. J.; Yang, G.; Weiss, M. S.; Liu, Y. J.; Chen, G. S.; Jiang, M. Protein Crystalline Frameworks with Controllable Interpenetration Directed by Dual Supramolecular Interactions. *Nat. Commun.* **2014**, *5*, 4634.

(24) Hou, C. X.; Li, J. X.; Zhao, L. L.; Zhang, W.; Luo, Q.; Dong, Z. Y.; Xu, J. Y.; Liu, J. Q. Construction of Protein Nanowires through Cucurbit[8]uril-Based Highly Specific Host-Guest Interactions: An Approach to the Assembly of Functional Proteins. *Angew. Chem.* **2013**, *125*, 5700−5703.

(25) Bai, Y. S.; Luo, Q.; Zhang, W.; Miao, L.; Xu, J. Y.; Li, H. B.; Liu, J. Q. Highly Ordered Protein Nanorings Designed by Accurate Control of Glutathione S-Transferase Self-Assembly. *J. Am. Chem. Soc.* **2013**, *135*, 10966−10969.

(26) Gao, X.; Yang, S.; Zhao, C. C.; Ren, Y. H.; Wei, D. Z. Artificial Multienzyme Supramolecular Device: Highly Ordered Self-Assembly of Oligomeric Enzymes *in Vitro* and *in Vivo*. *Angew. Chem.* **2014**, *126*, 1−5.

(27) Miao, L.; Han, J. S.; Zhang, H.; Zhao, L. L.; Si, C. Y.; Zhang, X. Y.; Hou, C. X.; Luo, Q.; Xu, J. Y.; Liu, J. Q. Quantum-Dot-Induced Self-Assembly of Cricoid Protein for Light Harvesting. *ACS Nano* **2014**, *8*, 3743−3751.

(28) Sun, H. C.; Zhang, X. Y.; Miao, L.; Zhao, L. L.; Luo, Q.; Xu, J. Y.; Liu, J. Q. Micelle-Induced Self-Assembling Protein Nanowires: Versatile Supramolecular Scaffolds for Designing the Light-Harvesting System. *ACS Nano* **2016**, *10*, 421−428.

(29) Medalsy, I.; Dgany, O.; Sowwan, M.; Cohen, H.; Yukashevska, A.; Wolf, S. G.; Wolf, A.; Koster, A.; Almog, O.; Marton, I.; Pouny, Y.; Altman, A.; Shoseyov, O.; Porath, D. SP1 Protein Based Nanostructures and Arrays. *Nano Lett.* **2008**, *8*, 473−477.

(30) Heyman, A.; Medalsy, I.; Or, O. B.; Dgany, O.; Gottlieb, M.; Porath, D.; Shoseyov, O. Protein Scaffold Engineering Towards Tunable Surface Attachment. *Angew. Chem., Int. Ed.* **2009**, *48*, 1−6.

(31) Wang, X. R.; Hu, J. M.; Zhang, G. Y.; Liu, S. Y. Highly Selective Fluorogenic Multianalyte Biosensors Constructed *via* Enzyme-Catalyzed Coupling and Aggregation-Induced Emission. *J. Am. Chem. Soc.* **2014**, *136*, 9890−9893.

(32) Hu, J. M.; Zhang, G. Q.; Liu, S. Y. Enzyme-Responsive Polymeric Assemblies, Nanoparticles and Hydrogels. *Chem. Soc. Rev.* **2012**, *41*, 5933−5949.

(33) Klostranec, J. M.; Chan, W. C. W. Quantum Dots in Biological and Biomedical Research: Recent Progress and Present Challenges. *Adv. Mater.* **2006**, *18*, 1953−1964.

(34) Medintz, I. L.; Uyeda, H. T.; Goldman, E. R.; Mattoussi, H. Quantum Dot Bioconjugates for Imaging, Labelling and Sensing. *Nat. Mater.* **2005**, *4*, 435−446.

(35) Dennis, A. M.; Bao, G. Quantum Dot-Fluorescent Protein Pairs as Novel Fluorescence Resonance Energy Transfer Probes. *Nano Lett.* **2008**, *8*, 1439−1445.

(36) Dennis, A. M.; Rhee, W. J.; Sotto, D.; Dublin, S. N.; Bao, G. Quantum Dot Fluorescent Protein FRET Probes for Sensing Intracellular pH. *ACS Nano* **2012**, *6*, 2917−2924.

(37) Tang, B.; Wang, Y. *Spectrochim. Acta, Part A* **2003**, *59*, 2867−2874.

(38) Tang, B.; Wang, Y.; Liang, H. L.; Chen, Z. Z.; He, X. W.; Shen, H. X. *Spectrochim. Acta, Part A* **2006**, *63*, 609−613.